IEEE Photonics Journal
An IEEE Photonics Society Publication

Open Access

An Amorphous $(Al_{0.12}Ga_{0.88})_2O_3$ Deep Ultraviolet Photodetector

Volume 12, Number 4, August 2020

Shu-Bai Liu
Shoou-Jinn Chang, *Fellow, IEEE*
Sheng-Po Chang, *Member, IEEE*
Chia-Hsun Chen

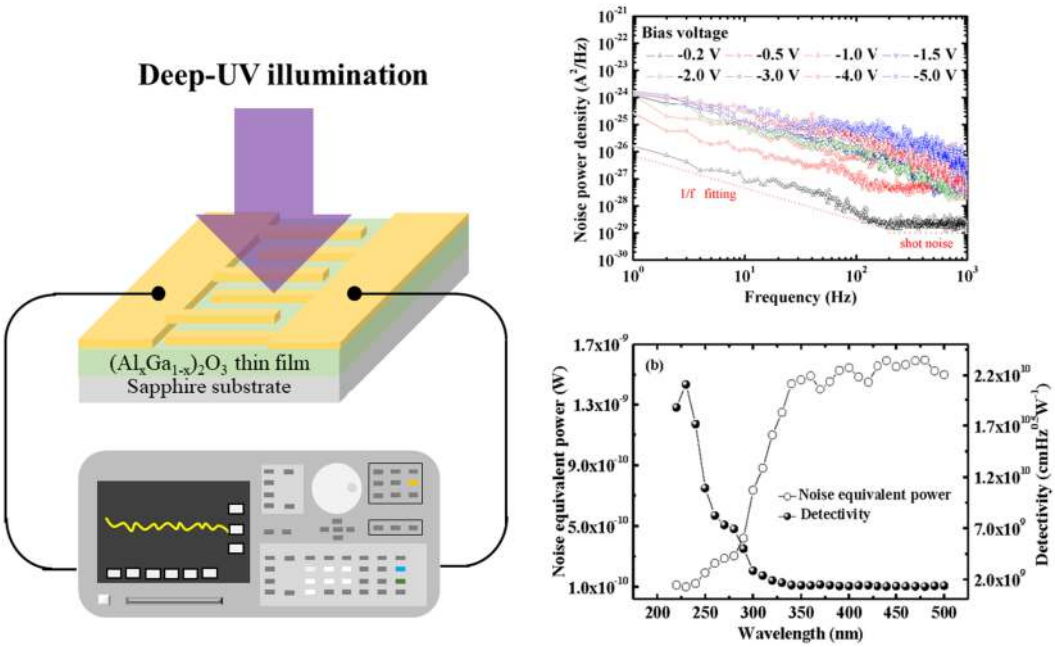

DOI: 10.1109/JPHOT.2020.3001582

An Amorphous $(Al_{0.12}Ga_{0.88})_2O_3$ Deep Ultraviolet Photodetector

Shu-Bai Liu,[1] Shoou-Jinn Chang ,[1] *Fellow, IEEE*, Sheng-Po Chang ,[1] *Member, IEEE*, and Chia-Hsun Chen[2]

[1]Institute of Microelectronics, Department of Electrical Engineering, Advanced Optoelectronic Technology Center, National Cheng Kung University, Tainan 70101, Taiwan
[2]Department of Optometry, Chung Hwa University of Medical Technology, Tainan 71703, Taiwan

DOI:10.1109/JPHOT.2020.3001582

Manuscript received May 12, 2020; revised June 2, 2020; accepted June 8, 2020. Date of publication June 12, 2020; date of current version July 8, 2020. This work was supported by the Ministry of Science and Technology, Taiwan, and Advanced Optoelectronic Technology Center, National Cheng Kung University for their financial support. (Corresponding author: Shoou-Jinn Chang (e-mail: changsj@mail.ncku.edu.tw).

Abstract: The authors report the deposition of an $(Al_xGa_{1-x})_2O_3$ amorphous thin film on sapphire substrates by sputter deposition. An amorphous deep ultraviolet (UV) $(Al_{0.12}Ga_{0.88})_2O_3$ photodetector, with a cutoff wavelength at 230 nm, was also fabricated. With -10 V applied bias, it was found the dark leakage current and the linear dynamic range (LDR) of the fabricated photodetector were about 1.23×10^{-9} A and 59.51 dB, respectively. With the same -10 V applied bias, the UVC/UVA contrast ratio was larger than 20. With $\lambda_{illumination} = 230$ nm and -5 V applied bias, it was found noise equivalent power (NEP) and detectivity (D^*) of the fabricated amorphous deep UV $(Al_{0.12}Ga_{0.88})_2O_3$ photodetector were 9.94×10^{-11} W and 2.11×10^{10} cmHz$^{1/2}$W^{-1}, respectively. These results suggest the fabricated amorphous deep UV $(Al_{0.12}Ga_{0.88})_2O_3$ photodetector herein indicate a cost-effective solution for developing DUV photodetector applications.

Index Terms: $(Al_xGa_{1-x})_2O_3$, wide-bandgap material, deep UV photodetector, amorphous.

1. Introduction

Ultraviolet (UV) photodetectors are important devices which can be used in various applications, such as missile warning, underwater communication, fire alarms, and chemical/biological sensing [1]–[4]. To effectively detect the UV radiation, one needs to use wide-bandgap semiconductors, such as GaN, ZnO, SiC, and their ternary and/or quaternary compounds. Among these materials, GaN can be epitaxially grown by metalorganic chemical vapor deposition (MOCVD) on sapphire substrate. This makes high quality GaN samples commercially available with reasonable price. It has been reported that GaN photodetectors can provide a larger UV responsivity [4]. For photodetector applications, it should be noted the 3.4 eV bandgap energy of GaN corresponds to a cutoff wavelength, λ cutoff, of 360 nm. In other words, GaN can only be used as a material for visible-blind photodetectors (i.e., 280 nm $< \lambda_{cutoff} <$ 400 nm), which also detect UV light emitted from the sun. Thus, high background and/or false detection might occur. To achieve solar-blind photodetectors (i.e., $\lambda_{cutoff} <$ 280 nm), one could use AlGaN alloys with a high Al content to serve as the active light absorption layer [5]–[8]. It was well-known the epitaxial layer quality will

deteriorate rapidly with increased Al, due to the high Al-content might cause the residual stresses occur in crystalline films, but still some previous study used some methods to improve the device characteristics. R. McClintock *et al*. reported a lateral silicon-indium conduction co-doping layer to achieve cracking free material and the unbiased EQE of 60% [9]. Recently, Anisha Kalra *et al*. first reported the polarization graded Mg-doped layer for p-i-n detectors to eliminate band discontinuities and reached highest responsivity value of 211mA/W at zero bias [10]. However, these methods were relative more complicated than directly deposited Ga_2O_3 and its compound on single crystal substrates which is lacking for III-nitrides.

Gallium oxide (Ga_2O_3) is an interesting material that has attracted much attention in recent years. With good thermal stability and a wide direct bandgap energy of 4.8-4.9 eV, λ_{cutoff} of Ga_2O_3 photodetectors occurs at around 260 nm. This make Ga_2O_3 photodetectors suitable for solar-blind photodetector applications. To our knowledge, Ga_2O_3 photodetectors prepared by pulse laser deposition (PLD) [11], MOCVD [12], [13], atomic layer deposition (ALD) [14], plasma-enhanced chemical vapor deposition (PECVD) [15], molecular beam epitaxy (MBE) [16], and furnace oxidation of GaN [17] have all been demonstrated.

Although it is possible to achieve true solar-blind photodetectors using Ga_2O_3 as the light absorption material, we still need to further push the cutoff wavelength, λ_{cutoff}, to even short wavelength region for applications such as space astronomy and solar research. For these applications, one can incorporate aluminum (Al) into the Ga_2O_3 film. The ternary $(Al_xGa_{1-x})_2O_3$ is an interesting material. By increasing the composition ratio of Al, we could increase the bandgap energy of $(Al_xGa_{1-x})_2O_3$ from 4.9 to 8.8 eV [18]. However, only few reports regarding the fabrication of $(Al_xGa_{1-x})_2O_3$ UV photodetectors could be found in the literature. For example, Weng *et al*. converted AlGaN into the $(Al_xGa_{1-x})_2O_3$ thin film by high temperature furnace oxidation and reported the fabrication of an $(Al_xGa_{1-x})_2O_3$ deep UV photodetector with a λ_{cutoff} of 220 nm [19]. The noise equivalent power (NEP) and detectivity (D*) of the $(Al_xGa_{1-x})_2O_3$ deep UV photodetector fabricated by furnace oxidation of AlGaN were also reported.

Very recently, Chen *et al*. reported the cost-effective sputter deposition of $(Al_xGa_{1-x})_2O_3$ polycrystalline thin film on sapphire substrate at high temperature (i.e., 600 °C) using the mixture of O_2 and Ar as the sputtering gas [20]. They investigated the effects of O_2 concentration on the structural, morphological, optical and compositional of the deposited $(Al_xGa_{1-x})_2O_3$ polycrystalline thin film. $(Al_xGa_{1-x})_2O_3$ deep UV photodetectors with a λ_{cutoff} of 230 nm were also fabricated [20]. They reported the on/off current ratio and peak responsivity of the fabricated photodetectors. Although NEP and D* are two important parameters for photodetectors, Chen *et al*. did not report the values of NEP and D* of their photodetector. In this study, we report the fabrication of an $(Al_xGa_{1-x})_2O_3$ amorphous deep UV photodetector prepared at room temperature, instead of at elevated temperature, by sputtering. The characteristics of the deposited $(Al_xGa_{1-x})_2O_3$ amorphous thin films and detailed performances of the fabricated amorphous $(Al_xGa_{1-x})_2O_3$ deep UV photodetectors, include NEP and D*, will also be discussed.

2. Experimental Details

The 110-nm-thick $(Al_xGa_{1-x})_2O_3$ amorphous thin film used in this study was prepared at room temperature by magnetron sputtering on both silicon and c-plane sapphire substrates using metallic Al (DC power = 70 Watt) and Ga_2O_3 (RF power = 100 Watt) targets. During deposition, mixture of O_2 and Ar was used as the sputtering gas while the chamber pressure was kept at 4×10^{-3} Torr. After the growth energy-dispersive X-ray spectroscopy (EDS) and X-ray diffraction (XRD) were used to characterize physical properties of the $(Al_xGa_{1-x})_2O_3$ thin film deposited on silicon substrate. On the other hand, the metal-semiconductor-metal (MSM) photodetector was fabricated using the $(Al_xGa_{1-x})_2O_3$ thin film deposited on sapphire substrate. To fabricate the deep UV photodetector, we deposited a thick Ni/Au (30/100 nm) film through an interdigitated shadow mask onto the $(Al_xGa_{1-x})_2O_3$ surface to serve as the contact electrodes. As shown in Fig. 1, the dimension of the interdigitated finger electrodes was 2 mm wide and 2.2 mm long, with finger width of 0.1 mm and spacing of 0.2 mm, respectively.

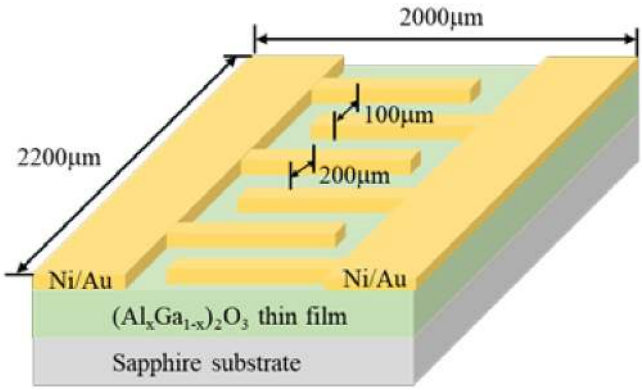

Fig. 1. Cross-sectional diagram of the fabricated $(Al_xGa_{1-x})_2O_3$ deep UV photodetector on sapphire substrates.

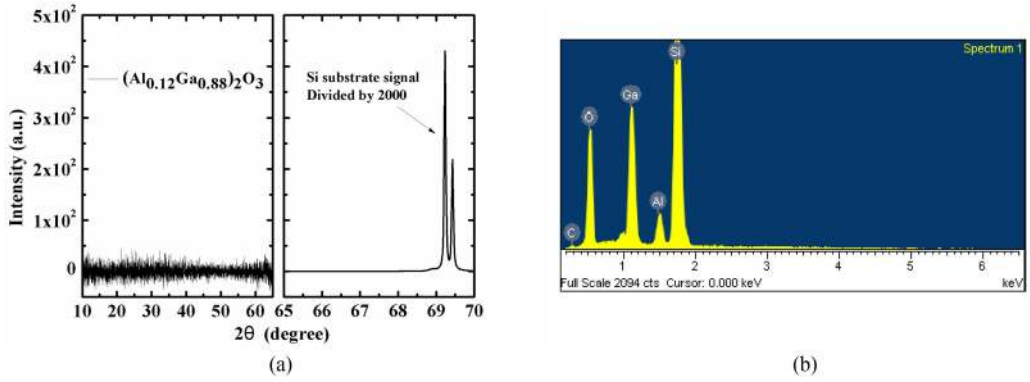

Fig. 2. (a) X-ray diffraction (XRD) and (b) Energy-dispersive X-ray spectroscopy (EDS) spectrum measured from the $(Al_xGa_{1-x})_2O_3$ thin film deposited on Si substrate.

Current-voltage (I-V) characteristics of the fabricated photodetector were then measured by an Agilent B1500 semiconductor parameter analyzer at room temperature. Spectral responsivity measurements of the photodetector were also performed by JOBIN-YVON SPEX System with a 300 W xenon arc lamp light source (PERKINELMER PE300BUV) and a standard synchronous detection scheme. During photocurrent measurements, the monochromatic light was guided by an optical fiber to illuminate the absorption layer of the $(Al_xGa_{1-x})_2O_3$ deep UV photodetector in the wavelength range from 220 nm to 500 nm.

3. Results and Discussion

XRD was first used to investigate the quality of the $(Al_xGa_{1-x})_2O_3$ thin film deposited on silicon substrate. Fig. 2(a) shows measured XRD pattern of the $(Al_xGa1\text{-}x)_2O_3$ thin film by Cu Kα source. As shown in the left side of Fig. 2(a), however, no clear peak was observed in the XRD spectrum between 2θ range of 10° to 65°. Only silicon substrate related peaks were observed at 69.2° and 69.4° in the right side of Fig. 2(a). Such a result indicates the room temperature deposited $(Al_xGa_{1-x})_2O_3$ thin film was indeed amorphous. EDS was subsequently used to estimate the Al content in the $(Al_xGa_{1-x})_2O_3$ thin film deposited on Si substrate. As shown in Fig. 2(b), Al, Ga, and O signals were clearly observed. The weak carbon signal was probably originated from the carbon adhesion film, contaminated during sample preparation. It was also found from the EDS result the Al: Ga atomic ratio was 12: 88 in the deposited $(Al_xGa_{1-x})_2O_3$ thin film. It has been reported

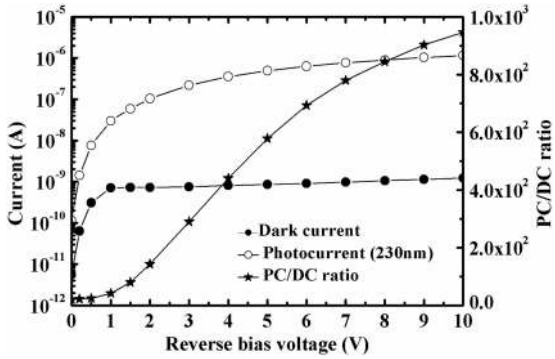

Fig. 3. I-V characteristics of the fabricated photodetector measured in dark and under illumination. PC/DC ratio as a function of the applied reverse bias was also plotted.

previously the bandgap energy of Ga_2O_3 and Al_2O_3 was 4.9 eV and 8.8 eV, respectively. It has been shown previously that bowing parameter, b, was about 0.32 for the ternary $(Al_xGa_{1-x})_2O_3$ [21], we can thus find that bandgap energy of the deposited $(Al_{0.12}Ga_{0.88})_2O_3$ was around 5.32 eV, using the Vegard's law:

$$E_g^{(Al_xGa_{1-x})_2O_3}(x) = (1-x)E_g^{Ga_2O_3} + xE_g^{Al_2O_3} + bx(1-x) \quad (1)$$

Fig. 3 shows I-V characteristics of the fabricated $(Al_{0.12}Ga_{0.88})_2O_3$ deep UV photodetector measured in the dark and under illumination. During photocurrent (PC) measurements, we illuminated the $(Al_xGa_{1-x})_2O$ photodetector with 230 nm UV light. With -10 V applied bias, it can be seen the measured dark current (DC) was only around 1.23×10^{-9} A. In contrast, PC was as high as 1.16×10^{-6} A, when measured with the same -10 V applied bias. Fig. 3 also shows the PC/DC ratio as a function of the applied reverse bias. As we increased the applied reverse bias, the high electric field applied on the device could result in a reduced probability of photo-generated carriers trapped by the localized states. Thus, the PC/DC ratio increased monotonically with the applied reverse bias. The linear dynamic range (LDR), defined as LDR = 20 log (PC/DC) [22]–[24], is an important figure-of-merit for the photodetector. From the data shown in Fig. 3, it was found the LDR under 230 nm irradiation was about 32.54 dB, 55.25 dB and 59.51 dB when the fabricated photodetector was biased at -1 V, -5 V and -10 V, respectively.

Fig. 4(a) shows measured spectral responses of the fabricated amorphous $(Al_{0.12}Ga_{0.88})_2O_3$ photodetector with various applied reverse bias voltages. Here, the responsivity is defined as $R(\lambda) = (PC-DC)/P(\lambda)$, where PC is the photocurrent, DC is the dark current and $P(\lambda)$ is the illumination power [25]. It was found the measured spectral response peaked at 230 nm, which corresponds to the bandgap energy of the deposited amorphous $(Al_{0.12}Ga_{0.88})_2O_3$ thin film. As we increased the wavelength of illumination light, it can be seen the measured responsivity decreased rapidly. In this study, we defined the ultraviolet C (UVC)/ultraviolet A (UVA) and the ultraviolet C (UVC)/visible contrast ratio as the responsivity measured at 230 nm to the responsivity measured at 380 nm of the UVA and at 450 nm of the visible illumination light, respectively. With these definitions, it could find the significant difference between two contrast ratios was small due to the defect or impurity state was rare in the amorphous $(Al_{0.12}Ga_{0.88})_2O_3$ thin film. As shown in the inset of Fig. 4(a), it can be seen the UVC/UVA contrast ratio was larger than 20 with a -10 V applied bias. Fig. 4(b) shows responsivity, $R(\lambda)$, and the corresponding external quantum efficiency, EQE, measured from the fabricated amorphous $(Al_{0.12}Ga_{0.88})_2O_3$ deep UV photodetector under various applied reverse bias voltages. During these measurements, we illuminated the photodetector with UVC light (i.e., $\lambda_{\text{illumination}} = 230$ nm). It should be noted the EQE can be determined using the

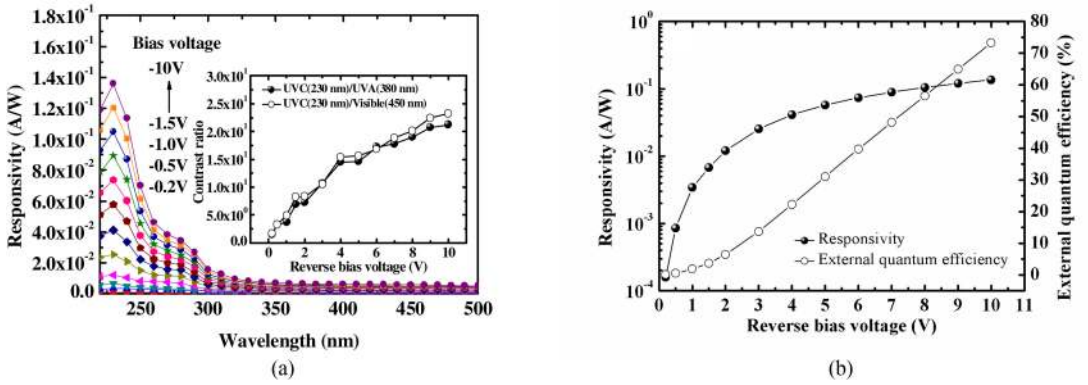

Fig. 4. (a) Spectral responsivity measured from the fabricated photodetector. The inset plotted the UVC/UVA contrast ratio. (b) The responsivity and external quantum efficiency of the fabricated photodetector under different reverse bias voltages.

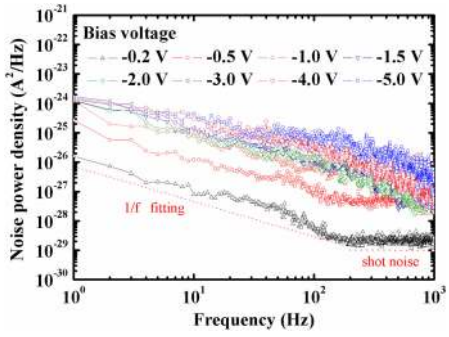

Fig. 5. Noise power density spectrum of the fabricated $(Al_{0.12}Ga_{0.88})_2O_3$ deep UV photodetector.

following formula [17], [26]:

$$\mathrm{EQE} = \mathrm{R}(\lambda) \times \frac{hc}{q\lambda} \tag{2}$$

where h is the Planck's constant, c is the speed of light in the vacuum, q is the elementary electron charge, and λ is the wavelength of the incident light. As we increased the applied reverse bias from -0.2 V to -5 V, it was found the peak photo response and thus the EQE increased rapidly. As we further increased the reverse bias, it can be seen the peak photo response and EQE kept increasing, however, with a slower speed. With -10 V applied bias and an incident light wavelength of 230 nm, it was found the responsivity of the fabricated amorphous $(Al_{0.12}Ga_{0.88})_2O_3$ photodetector was about 1.36×10^{-1} A/W, corresponds to an EQE about 73.26%.

In this study, the noise performance caused by the electric potential fluctuation in the deep UV photodetector was also measured by using the low noise current preamplifier (SR570) to measure the noise current. The noise power density spectrum of the SR570 amplified and extracted with the fast Fourier transform spectrum analyzer (Agilent 35670 dynamic signal analyzer) was shown in Fig. 5. It could be found the noise power density increased with the increasing applied reverse bias. In the frequency domain, the noise spectrum comprised various noise sources, including Johnson–Nyquist (thermal) noise ($S_{I,\mathrm{thermal}}$), shot noise ($S_{I,\mathrm{shot}}$) and flicker noise ($S_{I,\mathrm{flicker}}$). The current noise

power density (S_I) as a function of frequency could be expressed as the following equation:

$$S_I = S_{I,\text{thermal}} + S_{I,\text{shot}} + S_{I,flicker} = \frac{4KT}{R} + 2qI_d + S_0\frac{I_d^\beta}{f^\alpha} \tag{3}$$

where k is the Boltzmann constant, T is the absolute temperature, R is the resistance, q is the elementary electron charge, S_0 is the amplitude of the flicker noise, f is the frequency, α and β are two fitting parameters, and I_d is the dark current.

As shown in Fig. 5, the noise power density (NPD) spectrum measured at 300K can be decomposed into different components. At room temperature, the Johnson–Nyquist (thermal) noise should be negligibly small. On the other hand, the shot noise is independent of frequency while the flicker noise is inversely proportional to frequency. Thus, the flicker noise became dominate in the low frequency region. In the frequency range of 1 Hz to 100 Hz, the spectra measured in Fig. 5 can be well fitted by the Hooge-type equation. The value of α was found to be around 1, indicated the low frequency noise was dominated by flicker noise (1/f-type noise). In addition, the value of β was determined to be around 1.71 by the relationship of $S_{I,\text{flicker}}$ and I_d. Thus, we found the value of S_0 was around 4.13×10^{-9} for the fabricated photodetector. On the other hand, the mean square flicker noise current could be determined by integrated $S_{I,\text{flicker}}$. Thus, the total mean square noise current including the part of the shot noise and the flicker noise can be calculated by integrating the noise power density spectra:

$$\begin{aligned} &< i_n >^2 = \int_0^B S_I(f)df \\ &= \int_0^1 S_I(1)df + \int_0^B S_I(f)df = S_0[\ln(B) + 1] \end{aligned} \tag{4}$$

Here, we assume $S_I(f) = S_I(1Hz)$ for $f < 1$Hz and B is the bandwidth. With an applied reverse bias of -1 V, -3 V and -5 V, the mean square noise current $< i_n >^2$ over the bandwidth of 1k Hz was 7.8×10^{-24} A, 1.60×10^{-23} A, and 3.29×10^{-23} A, respectively. Using the data shown in Fig. 5 we can determine the NEP of our photodetector by using the equation [28], [29]:

$$\text{NEP} = \frac{\sqrt{< i_n^2 >}}{\text{R}(\lambda)} = \frac{\sqrt{< i_{n,\text{shot}}^2 > + < i_{n,flicker}^2 >}}{\text{R}(\lambda)} \tag{5}$$

where R(λ) is the responsivity.

We can also determine D* of the fabricated photodetector by substituting the NEP into the following equation [24], [25]:

$$\text{D}^* = \frac{\sqrt{\text{A}}\sqrt{\text{B}}}{\text{NEP}} \tag{6}$$

where A is the illumination area, and B is the bandwidth.

Fig. 6(a) and 6(b) show NEP and D* of the fabricated amorphous $(Al_{0.12}Ga_{0.88})_2O_3$ deep UV photodetector calculated using these equations measured with various applied reverse biases and various incident light wavelength, respectively. As shown in Fig. 6(a), the corresponding NEP under $\lambda_{\text{illumination}}$ at 230 nm was 8.15×10^{-10} W, 1.57×10^{-10} W, and 9.94×10^{-11} W under the applied biases of -1 V, -3 V and -5 V, respectively. Thus, the corresponding calculated D* at the same reverse bias voltage was 2.57×10^9 cmHz$^{1/2}$W^{-1}, 1.33×10^{10} cmHz$^{1/2}$W^{-1}, and 2.11×10^{10} cmHz$^{1/2}$W^{-1}, respectively. It was worth noted the NEP decreased as the applied reverse bias increased. In contrast, D* increased as we increased the applied reverse bias voltage.

Fig. 6(b) shows NEP and D* measured at -5 V applied bias with various wavelength. It can be seen the peak D* occurred at the wavelength of 230 nm, and decreased with the increase of the illumination light wavelength. On the other hand, NEP increased as we increased the illumination light wavelength from 220 nm to 350 nm. It should be noted the peak D* was around 2.11×10^{10} cmHz$^{1/2}$W^{-1}and occurred when $\lambda_{\text{illumination}} = 230$ nm with -5 V applied bias. Such a large D* indicates the amorphous $(Al_{0.12}Ga_{0.88})_2O_3$ photodetector is suitable for the detection of deep UV light. Using the same room temperature deposition conditions, we should be able

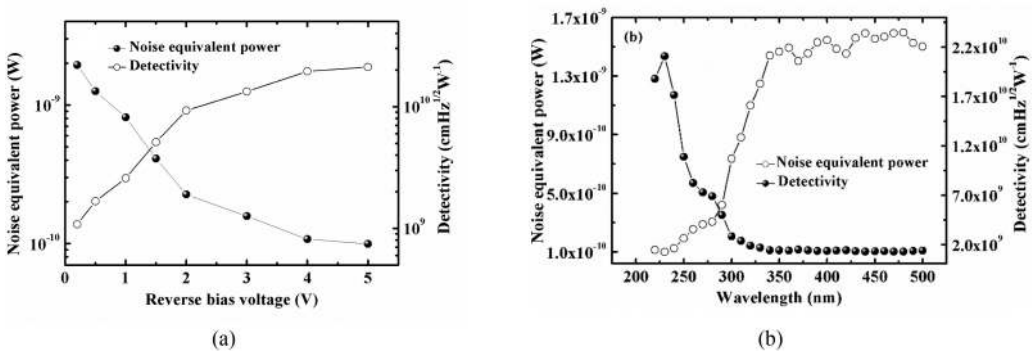

Fig. 6. (a) NEP and D* of the fabricated photodetector under different applied reverse bias voltages. (b) The NEP and D* calculated under the reverse bias of −5 V at various incident light wavelength.

to deposit the amorphous $(Al_{0.12}Ga_{0.88})_2O_3$ thin film on glass substrate and fabricate the deep UV $(Al_{0.12}Ga_{0.88})_2O_3$ photodetectors with the same performances. This could result in significant reduction of the production cost of the deep UV photodetectors.

4. Conclusion

In conclusion, we report the deposition of an $(Al_xGa_{1-x})_2O_3$ amorphous thin film on sapphire substrates by room temperature sputter deposition. An amorphous deep UV $(Al_{0.12}Ga_{0.88})_2O_3$ photodetector, with a cutoff wavelength at 230 nm, was also fabricated. With −10 V applied bias, it was found the dark leakage current and the LDR of the fabricated photodetector were about 1.23×10^{-9} A and 59.51 dB, respectively. With the same −10 V applied bias, it was found the UVC/UVA contrast ratio was larger than 20. Furthermore, it was found the NEP and D* of the fabricated amorphous deep UV $(Al_{0.12}Ga_{0.88})_2O_3$ photodetector were 9.94×10^{-11} W and 2.11×10^{10} $cmHz^{1/2}W^{-1}$, respectively, when the device was illuminated at 230 nm and biased at −5 V. These great characteristics of the fabricated amorphous deep UV $(Al_{0.12}Ga_{0.88})_2O_3$ photodetector herein indicate a cost-effective solution for developing DUV photodetector applications.

Acknowledgment

The authors wish to thank the Ministry of Science and Technology, Taiwan, and Advanced Optoelectronic Technology Center, National Cheng Kung University for their financial support.

References

[1] H. Shen, C. X. Shan, B. H. Li, B. Xuan, and D. Z. Shen, "Reliable self-powered highly spectrum-selective ZnO ultraviolet photodetectors," *Appl. Phys. Lett.*, vol. 103, no. 23, pp. 232112-1–232112-4, Dec. 2013.
[2] S. P. Chang *et al.*, "ZnO photoconductive sensors epitaxially grown on sapphire substrates," *Sensors Actuators A*, vol. 140, no. 1, pp. 60–64, Oct. 2007.
[3] S. J. Young, L. W. Ji, T. H. Fang, S. J. Chang, Y. K. Su, and X. L. Du, "ZnO ultraviolet photodiodes with Pd contact electrodes," *Acta Materialia*, vol. 55, no. 1, pp. 329–333, Jan. 2007.
[4] C. K. Wang *et al.*, "GaN MSM UV photodetectors with titanium tungsten transparent electrodes," *IEEE Trans. Electron. Devices*, vol. 53, no. 1, pp. 38–42, Jan. 2006.
[5] S. J. Chang, H. Hung, Y. C. Lin, M. H. Wu, H. Kuan, and R. M. Lin, "AlGaN ultraviolet metal-semiconductor-metal photodetectors with low-temperature-grown cap layers," *Jpn. J. Appl. Phys.*, vol. 46, no. 4B, pp. 2471–2473, Apr. 2007.
[6] W. Zhang *et al.*, "High-performance AlGaN metal semiconductor metal solar-blind ultraviolet photodetectors by localized surface plasmon enhancement," *Appl. Phys. Lett.*, vol. 106, no. 2, pp. 021112-1–021112-5, Jan. 2015.
[7] S. Rathkanthiwar *et al.*, "Gain mechanism and carrier transport in high responsivity AlGaN-based solar blind metal semiconductor metal photodetectors," *J. Appl. Phys.*, vol. 121, no. 16, pp. 164502-1–164502-10, Apr. 2017.
[8] P. Pramanik *et al.*, "Compositional inhomogeneities in AlGaN thin films grown by molecular beam epitaxy: Effect on MSM UV photodetectors," *J. Appl. Phys.*, vol. 120, no. 14, pp. 144502-1–144502-9, Oct. 2016.

[9] R. McClintock *et al.*, "High quantum efficiency AlGaN solar-blind p-i-n photodiodes," *Appl. Phys. Lett.*, vol. 84, no. 8, pp. 1248–1250, Feb. 2004.
[10] Y. Zhao and W. R. Donaldson, "Ultrafast UV AlGaN metal–semiconductor–metal photodetector with a response time below 25 ps," *IEEE J. Quantum Electron.*, vol. 56, no. 3, pp. 1–7, Jun. 2020.
[11] F. P. Yu, S. L. Ou, and D. S. Wuu, "Pulsed laser deposition of gallium oxide films for high performance solar-blind photodetectors," *Opt. Mater. Express*, vol. 5, no. 5, pp. 1240–1249, Apr. 2015.
[12] S. Oh, Y. Jung, M. A. Mastro, J. K. Hite, C. R. Eddy, Jr., and J. Kim, "Development of solar-blind photodetectors based on Si-implanted β-Ga_2O_3," *Opt. Express*, vol. 23, no. 22, pp. 28300–28305, Oct. 2015.
[13] G. C. Hu, C. X. Shan, N. Zhang, M. M. Jiang, S. P. Wang, and D. Z. Shen, "High gain Ga_2O_3 solar-blind photodetectors realized via a carrier multiplication process," *Opt. Express*, vol. 23, no. 10, pp. 13554–13561, May 2015.
[14] S. H. Lee *et al.*, "High-responsivity deep-ultraviolet-selective photodetectors using ultrathin gallium oxide films," *ACS Photon.*, vol. 4, pp. 2937–2943, Oct. 2017.
[15] Y. C. Chen *et al.*, "Ga_2O_3 photodetectors arrays for solar-blind imaging," *J. Mater. Chem. C*, vol. 7, pp. 2557–2562, 2019.
[16] O. Takayoshi, T. Okuno, and S. Fujita, "Ga_2O_3 thin film growth on c-plane sapphire substrates by molecular beam epitaxy for deep-ultraviolet photodetectors," *Japanese J. Appl. Phys.*, vol. 46, no. 11, pp. 7217–7220, Nov. 2007.
[17] W. Y. Weng, T. J. Hsueh, S. J. Chang, G. J. Huang, and H. T. Hsueh, "A β-Ga_2O_3 solar-blind photodetector prepared by furnace oxidization of GaN thin film," *IEEE Sensors J.*, vol. 11, no. 4, pp. 999–1003, Apr. 2011.
[18] B. W. Krueger, C. S. Dandeneau, E. M. Nelson, S. T. Dunham, F. S. Ohuchi, and M. A. Olmstead, "Variation of band gap and lattice parameters of $\beta-(Al_xGa_{1-x})_2O_3$ powder produced by solution combustion synthesis," *J. Am. Ceram. Soc.*, vol. 99, no. 7, pp. 2467–2473, Jul. 2016.
[19] W. Y. Weng *et al.*, "An $(Al_xGa_{1-x})_2O_3$ metal-semiconductor-metal VUV photodetector," *IEEE Sensor J.*, vol. 11, no. 9, pp. 1795–1799, Sep. 2011.
[20] P. W. Chen, S. Y. Huang, C. C. Wang, S. H. Yuan, and D. S. Wuu, "Influence of oxygen on sputtering of aluminum-gallium oxide films for deep-ultraviolet detector applications," *J. Alloys Compounds*, vol. 791, pp. 1213–1219, Jun. 2019.
[21] T. Wang, W. Li, C. Ni, and A. Janotti, "Band gap and band offset of Ga_2O_3 and $(Al_xGa_{1-x})_2O_3$ alloys," *Phys. Rev. Appl.*, vol. 10, no. 1, pp. 011003–1011003-7, Jul. 2018.
[22] X. Li *et al.*, "High detectivity graphene-silicon heterojunction photodetector," *Small*, vol. 12, no. 5, pp. 595–601, Feb. 2016.
[23] P. A. Hu *et al.*, "Highly responsive ultrathin GaS nanosheet photodetectors on rigid and flexible substrates," *Nano. Lett.*, vol. 13, no. 4, pp. 1649–1654, Mar. 2013.
[24] C. O. Kim *et al.*, "High photoresponsivity in an all-graphene p–n vertical junction photodetector," *Nat. Commun.*, vol. 5, pp. 4249-1–4249-7, Feb. 2014.
[25] R. Bhardwaj, P. Sharma, R. Singh, M. Gupta, and S. Mukherjee, "High responsivity $Mg_xZn_{1-x}O$ based ultraviolet photodetector fabricated by dual ion beam sputtering," *IEEE Sensors J.*, vol. 18, no. 7, pp. 2744–2750, Apr. 2018.
[26] Y. L. Wu *et al.*, "Ga_2O_3 nanowire photodetector prepared on SiO_2/Si template," *IEEE Sensors J.*, vol. 13, no. 6, pp. 2368–2373, Jun. 2013.
[27] E. Monroy, F. Calle, E. Munoz, F. Omnes, P. Gibart, and J. A. Munoz, "$Al_xGa_{1-x}N$:Si Schottky barrier photodiodes with fast response and high detectivity," *Appl. Phys. Lett.*, vol. 73, no. 15, pp. 2146–2148, Oct. 1998.
[28] Z. D. Huang *et al.*, "InGaN/GaN multiquantum-well metal-semiconductor-metal photodetectors with beta-Ga_2O_3 cap layers," *IEEE Sensors J.*, vol. 13, no. 4, pp. 1187–1191, Apr. 2013.
[29] Z. D. Huang, W. Y. Weng, S. J. Chang, C. J. Chiu, T. J. Hsueh, and S. L. Wu, "Ga_2O_3/AlGaN/GaN heterostructure ultraviolet three-band photodetector," *IEEE Sensors J.*, vol. 13, no. 9, pp. 3462–3467, Sep. 2013.